Characterisation of a transitionally occupied state of domain 1.1 of σ^{A} factor of RNA polymerase from *Bacillus subtilis*

Dávid Tužinčin[a,b], Petr Padrta[b], Kateřina Bendová[a,b], Libor Krásný[c], Lukáš Žídek[a,b], and Pavel Kadeřávek[b]

[a]National Centre for Biomolecular Research (NCBR), Faculty of Science, Masaryk University, Kamenice 5, 62500 Brno, Czech Republic; [b]Central European Institute of Technology (CEITEC), Masaryk University, Kamenice 5, 62500 Brno, Czech Republic; [c]Laboratory of Microbial Genetics and Gene Expression, Institute of Microbiology, Czech Academy of Sciences, CZ-14220 Prague 4, Czech Republic

This manuscript was compiled on July 26, 2022

σ factors are essential parts of bacterial RNA polymerase (RNAP) as they allow to recognize promotor sequences and initiate transcription. Domain 1.1 of vegetative σ factors occupies the primary channel of RNAP and also prevents binding of the σ factor to promoter DNA alone. Here, we show that domain 1.1 of *Bacillus subtilis* σ^{A} exists in two structurally distinct variants in dynamic equilibrium. The major conformation at room temperature is represented by a previously reported well-folded structure solved by nuclear magnetic resonance (NMR), but 4 % of the protein molecules are present in a less thermodynamically favorable state. We show that this population increases with temperature and may represent as much as 20 % at 43.5 °C. We characterized the minor state of the domain 1.1 using specialized methods of NMR. We found that, in contrast to the major state, the detected minor state is partially unfolded. Its propensity to form secondary structure elements is especially decreased for the first and third α helices, while the second α helix and β strand close to the C-terminus are more stable. In summary, this study reveals conformational dynamics of domain 1.1 and provides a basis for studies of its interaction with RNAP and effects on transcription regulation.

σ^{A} factor | RNA polymerase | *Bacillus subtilis* | NMR | conformational exchange

Introduction. Transcription of DNA into RNA performed by RNA polymerase (RNAP) is a key process in any living organism. Unlike in eukaryotes, there is only a single type of RNAP in bacteria. It is an enzyme composed of several subunits. The RNAP core present in Gram-negative bacteria is composed by five subunit (2α, β, β', ω) and two additional subunits δ and ϵ were identified in Gram-positive bacteria (1).

The RNAP core alone is able to elongate the transcription, but it is not capable of its initiation without a σ factor. The σ factors are essential for recognition of the promoter sequence, subsequent binding of RNAP to a promoter DNA, and beginning of the transcription process (2). The recognized crucial role of σ subunits in the transcription process was used to develop new antibacterial drugs (3).

The numbers of different σ factors are different in various species. There are species with only a single σ factor, but also with more than 100 different σ factors (4). The σ factors are divided according to their structure into groups σ^{70} and σ^{54}. There are no sequential similarities between these two groups and there is also another significant difference between these two families. The factors from the σ^{54} family require binding ATP activators (5) in contrast to σ^{70} factors. The σ^{70} factors are present in all bacterial species and they are divided into four groups according to their domain composition. Vegetative σ factors essential for transcription of housekeeping genes are classified into group 1 (σ^{70} in *Escherichia coli*, σ^{A} in *Bacillus subtilis*). The groups 2 to 4 contain σ factors dedicated to transcriptions of genes expressed upon an environmental stress (4, 5).

The σ factors of the first group are composed of four domains: domain 1.1, domain 2 (regions 1.2 – 2.4), domain 3 (regions 3.0 – 3.2), and domain 4 (regions 4.1 – 4.2). Regions 2.4 and 4.2 are critical for both formation of closed complex, i.e., the initial stage of binding of RNAP to DNA, and for formation of the transcription bubble called open complex, because they are recognizing −10 and −35 promoter consensus hexamers. Region 1.2 affects the stability of the transcription bubble by an interaction with DNA between the transcription start site (+1) and the −10 hexamer. Domain 3 binds to the −10 extended motif (TGx) preceding the −10 hexamer in some promotors and serves to increase the affinity of RNAP to promotor resulting in enhancement of transcription (4).

The domain 1.1 exhibits a specific autoregulation function as it inhibits the binding of the σ factor to DNA alone. The domain 1.1 of σ^{A} bound to free RNAP occupies the DNA binding channel (6, 7). The structure of domain 1.1 from *B. subtilis* consists of three α helices forming a hydrophobic core and of two short β strands arranged in a parallel β sheet (8). The secondary structure composition is similar to previously studied domain 1.1 from *Thermotoga maritima* (9). However, the structures of these two domains differ despite the sequence similarities. The first helix in the sequences has a significantly different orientation in these two structures. Surprisingly, the arrangement of the helices forming the hydrophobic core of the domain 1.1 from *B. subtilis* is similar to domain 1.1 from *Escherichia coli* (6) solved by X-ray crystallography in complex with RNAP and to the structured domain of RNAP δ subunit from *B. subtilis* (10). The structure of domain 1.1 from *B. subtilis* was shown to be affected by dynamics at the μs–ms timescale, typical for larger structure rearrangement (8). It was hypothesized (8) that the determined structure of the domain 1.1 from *B. subtilis* is in an exchange with a structure similar to domain 1.1 from *T. maritima*. Therefore we decided to obtain detailed information about the low populated state of the *B. subtilis* with atomistic resolution. The results presented here then reveal details of the dynamic equilibrium between the two states, its dependence on temperature, and biological implications.

Table 1. Comparison of the fitted global exchange parameters at different temperatures to the dispersion profiles, the error represents the 99% confidence level estimated from Monte-Carlo simulations.

T(°C)	k_{ex} (kHz)	p_B (%)	reduced χ^2
30	1.24 ± 0.01	8.2 ± 0.1	2.7
25	1.05 ± 0.02	3.87 ± 0.04	1.8
20	0.91 ± 0.01	2.18 ± 0.02	2.0
15	0.81 ± 0.02	1.30 ± 0.02	3.7
10	0.76 ± 0.04	0.78 ± 0.02	3.3
5	0.91 ± 0.08	0.43 ± 0.02	4.5
1	1.1 ± 0.2	0.28 ± 0.03	2.0

Results and Discussion.

Characterization of σ1.1 conformational exchange. Our first goal was to determine the quantitative parameters of the previously reported exchange in the backbone of the *B. subtilis* σ1.1 domain (8). We analyzed data provided by NMR experiments based on the Carr, Purcell, Meiboom and Gill pulse sequence (CPMG experiments)(11, 12). Using the CPMG approach, we measured how exchange between conformational states contributes to the relaxation of the signal corresponding to the magnetization of ^{15}N in the protein backbone. The experiments were performed at seven temperatures ranging from 1 °C to 30 °C. The exchange contribution to the relaxation rate at higher temperatures resulted in a significant attenuation of the NMR signal, preventing a detailed analysis of the CPMG data. At 25 °C, we detected exchange increasing the relaxation rates by at least 2.5 s^{-1} for 47 out of 71 analyzed amide ^{15}N signals. Results are summarized in Supporting information Table S1. The simplest two state model of the exchange reproduced the data well. The results of the analysis of the CPMG data of individual residues show similar values of kinetic and thermodynamic parameters suggesting that they report the same exchange event. In order to test this hypothesis, we tried to fit the available data of residues exhibiting the significant exchange together to obtain a single value of the exchange contribution k_{ex} and of the population of the minor state p_B for all residues at each temperature (Table 1). The population of the minor state ranged from approximately 8 % at 30 °C to less than 0.5 % at low temperatures (1 °C and 5 °C). The very low populations at low temperatures resulted in small exchange contributions which were difficult to analyze as indicated by a larger χ^2 parameter of the fit at 5°C. A smaller χ^2 obtained at 1°C cannot be attributed to an improved quality of the fit but to a lower precision of the input data due to the low signal to noise ratio in NMR spectra. Therefore, parameters determined at low temperatures should be interpreted with caution. An increased χ^2 parameter was also observed at 30°C. In addition, we detected two residues (A35 and F54) which can not be included in the global fit at 30°C, in contrast to the lower temperatures. It indicates that the dynamics is becoming more complicated and the application of two-state model may not be applicable at higher temperatures. Such a trend is expected because higher temperatures usually enhance population of additional states which can be safely neglected at lower temperatures. However, the significant drop of quality of NMR spectra at higher temperatures did not allow us to study the dynamics beyond the two-state model.

Despite the mentioned limitations, the determined populations follows the Boltzmann's law at the temperatures 10 – 25°C. We determined the enthalpy $\Delta H = (79 \pm 10)\,\mathrm{kJ\,mol^{-1}}$ and entropy $\Delta S = (0.24 \pm 0.03)\,\mathrm{kJ\,K^{-1}\ mol^{-1}}$ differences between the major and minor state from the temperature dependence of the equilibrium constant K (Figure 1a). In addition, we determined the thermodynamic parameters for reaching the transition saddle point on the free energy landscape from the major ($\Delta H_{AB} = (90 \pm 16)\,\mathrm{kJ\,mol^{-1}}$, $\Delta S_{AB} = (0.09 \pm 0.06)\,\mathrm{kJ\,K^{-1}\ mol^{-1}}$) and minor state ($\Delta H_{BA} = (14 \pm 6)\,\mathrm{kJ\,mol^{-1}}$, $\Delta S_{BA} = (-0.14 \pm 0.02)\,\mathrm{kJ\,K^{-1}\ mol^{-1}}$) from the temperature dependence of the forward and backward rate constants (Figure 1b,c). Extrapolation of the data to higher temperatures revealed that the low populated state accounted for cca. 12% and 20% at 37.0°C and 43.5°C, respectively.

Structural analysis of the minor state. The NMR structure determination of proteins is most typically based on inter-atomic proton-proton distances estimated from measured nuclear Overhauser effect (NOE) (13). As supplementary structural information, chemical shifts of backbone nuclei and occasionally scalar couplings or residual dipolar couplings (RDCs) (14) are used. Unfortunately, the portfolio of available methods for structure determination of low populated states of proteins in an exchange with their major state is more limited. It lacks the most fruitful source of structural information, i.e., the inter-atomic distance. Therefore, structural analysis of minor states relies mostly on the chemical shifts and RDCs.

Chemical shifts depend on the local electronic environment of individual nuclei and therefore provide atom-specific structural information. The chemical shifts of minor protein states with populations of a few percent and (sub)millisecond exchange times are not observed directly in NMR spectra (15, 16). Despite that, NMR spectra of these states can be reconstructed from

D.T. and K.B. prepared NMR samples, D.T. and P.K. measured NMR spectra, D.T., P.P., and P.K processed the spectra, D.T. and P.K. perform the analyses, D.T., L.Z., L.K., and P.K prepared the manuscript, P.K. obtained funding for the project.

The authors declare no conflict of interest.

The data that support the findings of this study are available from the corresponding author upon reasonable request.

[2] The correspondence should be addressed to E-mail: pavel.kaderavekmail.muni.cz

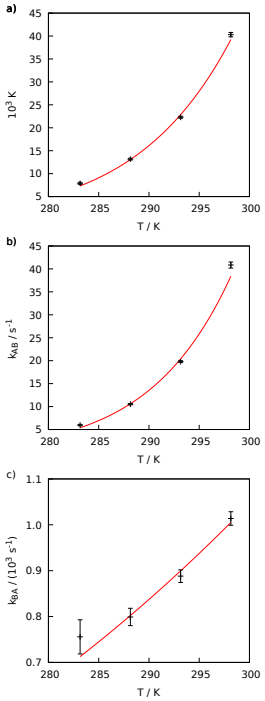

Fig. 1. The dependence of equilibrium constant K (a), forward k_{AB} (b), and backward k_{BA} (c) rate constants on temperature.

resonance frequencies of the major state, and chemical shift differences between states derived from CPMG experiments and/or chemical exchange saturation transfer (CEST) measurements (see Material and Methods). The detected changes of chemical shifts may be used to map the effects of the exchange on the structure.

Using CPMG and CEST experiments for different nuclei, we were able to obtain nearly complete ^{15}N, ^{13}C$^{\alpha}$, ^{13}CO, ^{1}HN backbone chemical shifts (Table S2 in Supporting information), as well as $|\Delta\omega|$ (difference between chemical shifts of major and minor state) of ^{13}C methyl side-chain chemical shifts (Table S3 in Supporting information). We then combined the chemical shift changes of backbone nuclei to a single parameter $\Delta\omega_{\mathrm{CSP}}$, referred to as the chemical shift perturbance (Eq. 5 in Material and Methods).

Figure 2 shows a structure of the major conformation of σ1.1 color-coded according to the values of $\Delta\omega_{\mathrm{CSP}}$ for residues with the chemical shift changes evaluated for all four backbone nuclei (residues 11–65). The negligible chemical shift perturbance of flexible termini documents a similar distribution of conformations in both states of the σ1.1 domain. Therefore, we assume that the termini retain the native structure. The highest $\Delta\omega_{\mathrm{CSP}}$ values were obtained for the residues 18, 20, 28, 31, 32, 47, 52, 56, and 65 suggesting that these residues are in a much different local environment in the minor vs. major state.

Positions of the methyl groups are also depicted in Figure 2 and color-coded according to $|\Delta\omega|$. In proteins, methyl groups are sensitive indicators of structure and dynamics (17) and they often report on events within the hydrophobic core. The CPMG experiments measured with σ1.1 samples including stereospecifically labeled methyl groups provided us a complete set

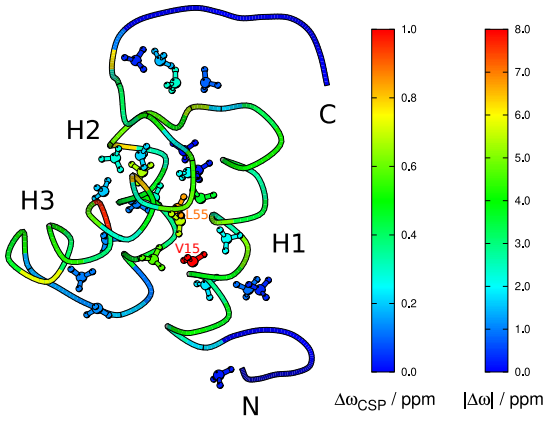

Fig. 2. The structure of the major state of σ1.1 (PDB 5MWW) color coded according to the size of backbone $\Delta\omega_{\mathrm{CSP}}$ (colored backbone) and methyl $|\Delta\omega|$ (colored models of CH3 groups) determined for the minor state. The red and orange CH_3 models correspond to pro-S methyl of V15 and pro-R methyl of L55, respectively.

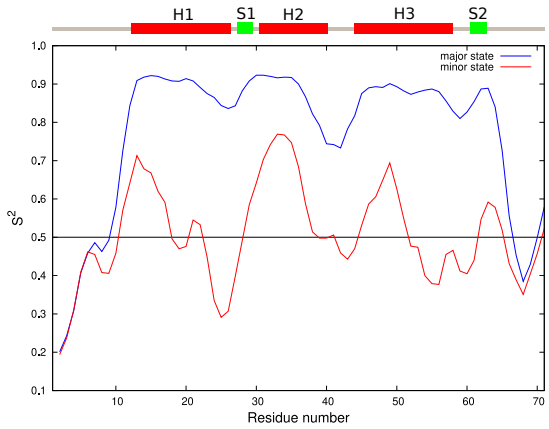

Fig. 3. Dependence of the estimated order parameter S^2 based on RCI approach calculated for the major (red) and minor (blue) states of σ1.1.

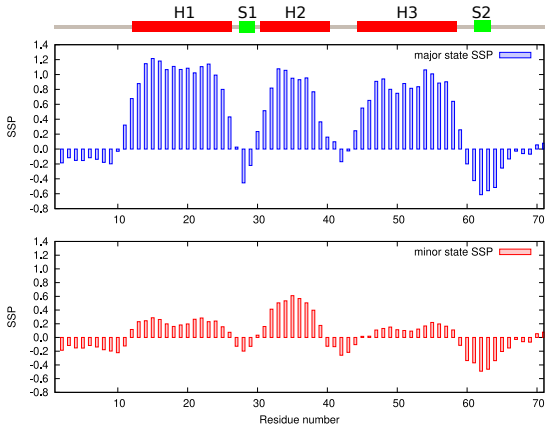

Fig. 4. Secondary structure propensity prediction calculated for major state (top, blue), and minor state (bottom, red). Secondary structures of major state are shown above the graph, helical structures are in red, beta sheets structures are in green.

of ^{13}C methyl chemical shifts of the minor state. The most significant changes were identified for Cγ-proS of V15, Cδ-proS of L19, both methyls in I34, and Cδ-proR of L55. All these methyls are located in a proximity of aromatic rings in the major state (Cγ-proS of V15 is close to F41, other mentioned methyls are in the proximity of Y51). It can be expected that the significant disturbance of their chemical shifts is induced by a change of the distance and orientation to the aromatic rings, known for a strong effect on the chemical shifts (18). Generally, the results indicate a larger structural rearrangement affecting the hydrophobic core of the σ1.1 structure.

Partial disorder of the minor state. The backbone chemical shift are very sensitive to the secondary structures. A lower dispersion of backbone amide proton chemical shifts (Figure S1 in Supporting information) indicates lower tendency of the minor state to form secondary structures. Comparison of chemical shifts of all backbone nuclei with their random-coil values (Figure S2 in Supporting information) confirmed that the chemical shift changes can be interpreted as a consequence of lower propensity of the minor state to form secondary structure.

Backbone chemical shifts also allowed us to predict the order parameters S^2, measuring angular amplitudes of motion for the backbone amide groups. The values estimated by the RCI approach (19), plotted in Figure 3, were lower for the minor state, in agreement with the lower content of secondary structures. The S^2 values indicate that the minor state exhibits higher flexibility (compared to the major state) in the regions corresponding to helix 1 (residues F12–R26), helix 3 (residues S45–E57) and β-sheet 1 (residues V28–T30). The N-termini (amino acids A1–T11) and the C-termini (amino acids S64–D71) remain flexible in both states.

In order to quantify the tendency to form the secondary structures, the parameter secondary structure propensity (SSP) (20) was calculated from chemical shifts of both states. SSP combines chemical shifts from different nuclei (in this case, all aforementioned backbone nuclei) into single score representing the expected tendency of a residue to form α-helical (positive value) or extended structure (negative value). The results are presented in Figure 4. Compared to the SSP of the major state, overall decrease in propensity to form secondary structure is observed across all structural elements of the minor state. However, SSP is not uniform in the minor state. The strongest tendency to form secondary structures was observed for helix 2 and for the β-sheet. The minor state is obviously far from a random coil conformation. Instead, it can be characterized as an ensemble of rapidly inter-converting substates (not resolved on the μs–ms time scale probed by our experiments). The

ensemble is dominated by conformation with a folded central region, consisting of helix 2 and the adjacent β-sheet. This conclusion is supported by RDCs measured for both states as shown is Supporting information Figure S3 and S4. Whereas RDCs determined for the major state are in a good agreement with the previously solved structure (8), RDCs of the minor state are more scattered, but far from a profile expected for a disordered protein (21).

Our investigation of the low populated state of the domain 1.1 is one of a very limited number of studies of excited states of proteins. Currently, NMR is the only method which allows us to determine temporarily present structures with population of few percent in a dynamic exchange with the major state. Nevertheless, NMR methods developed for this purpose (22, 23) provide a fruitful insight into possible conformational adaptability of proteins and the minor states may represent biologically interesting transition states accessed during a ligand binding or may play a role in a binding controlled by a conformational selection. What is a possible role of the minor state in the biological function of σ1.1? The minor state with lower SSP could be interpreted as a small fraction of unfolded σ1.1 domain. However, the less structured nature of the minor state does not exclude its physiological function. Currently, intrinsically disordered proteins are fully accepted as a functional part of the proteome with unique biophysical properties allowing them to play various roles requiring high flexibility and access to a larger conformational space than occupied by rigid proteins.

Here, we have defined the low populated state of the σ1.1 domain, and shown that its percentage markedly increases with increasing temperature. The excited structure of the σ1.1 domain is more disordered than the major state. Notably, there is no crystal structure of RNAP with the σ^{A} subunit from *B. subtilis* available and a weak electron density map of σ1.1 in the crystal structure of RNAP from *E. coli* indicates that σ1.1 is highly mobile in the holoenzyme (7). The inherent tendency of σ1.1 to form a less ordered state, observed in our study, has potential biological implications. It suggests that this conformational plasticity affecting the hydrophobic core is important for entry/exit of this domain into/from the primary channel of RNAP. This hypothesis is consistent with a recent study that investigated effects of the point mutation I48S in σ^{70} on transcription in *E. coli* (24), where a disturbance of the hydrophobic core of the protein resulted in significant phenotypic changes compared to the wild-type. Although the mutated residue I48 is weakly conserved in primary σ factors, it is often replaced with leucine or valine with similar biophysical properties. In *B. subtilis* this position corresponds to L55, which is located in the C- terminal α helix and its sidechain was shown in our study to be highly affected by the conformational exchange (Figure 2 and Table S3 in Supporting information). A parallel can be found also with the ω subunit of RNAP, where its flexibility is essential for its function, and even silent mutations (mutations that do not change amino acids but codons; subsequently, due to differential availability of aminoacylated tRNAs, the protein is folded differently) that reduce this flexibility compromise its interplay with RNAP and its biological function (25).

The higher tendency of the minor state to form α helix 2 and the β-sheet suggests that these secondary structure elements represent a core of the σ1.1 structure. Interestingly, the less ordered helices 1 and 3 interact in *E. coli* RNAP holoenzyme with an α helix in a linker between domains 1.1. and 1.2, and with the Gp2 inhibitor produced by the bacteriophage T7 (6). Helices 1 and 3 are oriented towards to the β' clamp whose motion was proposed to eject σ1.1 from the RNAP cleft (26).

Conclusions. We characterized a previously detected low populated state of the σ1.1 domain from RNA polymerase of *Bacillus subtilis*. Its population is about 4 % at 25 °C undergoing an exchange with the major state at the rate of approximately 1 kHz. The determined thermodynamic parameters predict an increase of the population of the minor state with the increasing temperature, reaching 20 % at 43.5 °C. The previously suggested hypothesis (8) that the excited state of the σ1.1 domain from *B. subtilis* is similar to another known structure of σ1.1 domain from *T. maritima* appears to be incorrect. Instead, the studied minor state was identified to be more flexible than the major state and it has a lower propensity to form a structured conformation, especially for helices 1 and 3. We hypothesize that the conformational plasticity of σ1.1 plays a role in binding and ejection of the domain 1.1 from the binding channel of RNAP.

Material and methods.

A. Sample preparation. Cloning procedure of gene encoding σ1.1 was described elsewhere (8). Expression, purification, and composition of samples are described in Supporting information. A purity and stability of the samples was verified prior every NMR measurement. A special attention was payed to avoid a contamination of glycerol which increases viscosity of the solvent and affects the measured relaxation rates. Four samples of wild-type σ1.1 were prepared in this study, each differing in the isotopic labeling scheme. The first sample was uniformly labeled with ^{15}N, ^{13}C in a protonated solvent. The second sample was uniformly labeled with ^{15}N and contained ^{1}H at all exchangeable positions, in addition, ^{13}C and ^{1}H were incorporated into methyl groups of Thr, Met and pro-S Leu, Ile and Val residues (27). All other positions contained ^{2}H and ^{12}C. The third sample was prepared in the same way as the second one, with the exception of ^{13}C and ^{1}H being incorporated in different methyl groups of Ala and pro-R Leu, Ile and Val residues (28). The fourth sample contained ^{2}H at all exchangeable positions and was labeled selectively at the $^{13}C^{\alpha}$ positions with the exception of Ile, Leu, and Val, where $^{13}C^{\beta}$ was partially enriched (29). All other positions contained natural abundance of ^{1}H and ^{12}C.

B. CPMG/CEST measurements. All NMR experiments were performed using Bruker Avance Neo spectrometers. The ^{15}N single-quantum relaxation dispersion experiments were performed on ^{13}C, ^{15}N uniformly labeled sample at 1 °C, 5 °C, 10 °C, 15 °C, 20 °C, 25 °C, and 30 °C using NMR spectrometers operating at proton frequencies of 600 MHz and 850 MHz, equipped with cryogenically cooled TCI probes. The ^{15}N CPMG experiment was performed in a relaxation compensated version (30), with optimized phase cycles applied to ^{15}N CPMG refocusing pulses (31). Backbone amide ^{15}N-^{1}H residual dipolar

couplings of the minor conformation were obtained by measuring a set of CPMG relaxation dispersion experiments (TROSY, anti-TROSY and continuous wave CPMG (32)) on partially aligned samples at 25 °C at 600 MHz (equipped with a cryogenically cooled TCI probe), 700 MHz (equipped with a cryogenically cooled TXO probe), and 850 MHz (equipped with a cryogenically cooled TCI probe). The maximum CPMG frequency was 1 kHz and the CPMG relaxation delay was set to 36 ms in all ^{15}N CPMG experiments. Alignment was achieved using Pf1 phage (33) (approximately 18 mg/ml, ALSA Biotech) and PEG (C12E5)/hexanol media (34). The analysis of CPMG experiments measured with alignment media were complemented with experiments for measurement of the amide ^{15}N longitudinal relaxation rates and relaxation rates of two-spin order (32) of the amide ^{15}N-^{1}H spin pair. Residual dipolar couplings of the major state conformation were measured using the IPAP approach (35). ^{15}N chemical shifts of the minor state were verified by a CEST experiment (36) performed at a 950 MHz spectrometer equipped with a cryogenically cooled TCI probe using ^{15}N labeled NMR sample. The CEST experiment was measured with the relaxation delay $T_{\mathrm{EX}} = 0.4$ s and irradition with ^{15}N B_1 field amplitude 29 Hz. The ^{15}N carrier frequency was set to 118.5 ppm and the CEST irradiation offset ranged from −1800 Hz to 1650 Hz with 25 Hz steps. Values of ^{13}C$^{\alpha}$, ^{13}CO, ^{1}HN chemical shifts of the minor state have been derived from CEST-based experiments (37–40). The ^{13}CO CEST experiment (39) was performed at the 700 MHz spectrometer equipped with a cryogenically cooled TXO probe with the ^{13}C and ^{15}N uniformly labeled sample, the CEST irradiation with the B_1 field amplitude 32 Hz was applied during the $T_{\mathrm{EX}} = 0.4$ s period. The ^{13}C carrier was set to 178.7 ppm and the CEST irradiation offsets ranged from −1400 Hz to 1400 Hz with spacing of 25 Hz. The ^{13}C$^{\alpha}$ CEST experiment (37) was performed at the 700 MHz spectrometer equipped with a cryogenically cooled TXO probe with the specifically labelled ^{13}C$^{\alpha}$ sample and at the 700 MHz spectrometer equipped with a cryogenically cooled TCI probe with uniformly ^{15}N and ^{13}C labeled sample using a different variant of the CEST experiment (38) with detection in the form of ^{1}H-^{15}N correlation spectra. The identical length of the CEST irradiation period $T_{\mathrm{EX}} = 0.4$ s was used in all ^{13}C$^{\alpha}$ CEST experiments together with the CEST irradiation offsets ranging from −2050 Hz to 2100 Hz with 50 Hz spacing. The CEST experiment performed with the specifically labeled sample was measured with the CEST ^{13}C B_1 irradiation field amplitude 26 Hz, the ^{13}C carrier frequency was set to 57 ppm. The ^{13}C$^{\alpha}$ CEST experiment measured with the uniformly labeled sample was performed with the CEST ^{13}C B_1 field of 30 Hz and the ^{13}C carrier frequency was set to 58 ppm. The same experiment was repeated with the setup adjusted for glycine residues with the CEST ^{13}C B_1 field amplitude 31 Hz, the ^{13}C carrier frequency set to 43.4 ppm and the CEST irradiation ^{13}C offsets ranging from −1250 Hz to 1600 Hz with spacing of 25 Hz. The amide proton chemical shifts were determined based on CEST experiments measured using selective pulse excitation (40) of sweep width 1200 Hz and 1250 Hz and with 3 excitations elements in the used waveform. All measurements of proton CEST were carried out on the 850 MHz spectrometer with the proton carrier frequency set to the water frequency (4.7 ppm) and the CEST irradiation of the length $T_{\mathrm{EX}} = 0.8$ s with offsets ranginging from 2605 Hz to 3855 Hz with 25 Hz step. The first proton CEST experiment with the amplitude of the CEST irradiation 29 Hz was performed with the deuterated sample containing specifically labeled methyl positions at Thr, Met and pro-S Leu, Ile and Val residues. The second experiment was performed with the B_1 field amplitude 25 Hz using the uniformly ^{15}N labeled sample to improve the analysis for residues which signal intensities in the ^{1}H-^{15}N correlation spectra were attenuated in the previous experiment due to the specific labeling. Methyl relaxation dispersion experiments were performed with samples specifically labeled at methyl positions using the Pf1 phage as an alignment medium (33) (approxmately 18 mg/ml, ALSA Biotech). The spin state selective and continuous wave CPMG experiments (41) were run at the 850 MHz (equipped with a cryogenically cooled TCI probe) and 700 MHz (equipped with a cryogenically cooled TXO probe) NMR spectrometers with the relaxation delay 30 ms and maximum CPMG frequency 1500 Hz. The sign of the change of the methyl chemical shift was estimated by a comparison of HSQC and HMQC spectra (42).

C. Data analysis. Data acquired from NMR measurements were converted and processed using the software NMRPipe (43), non-uniformly sampled data were processed using NMRPipe, version 9.9, and SMILE 2.0beta. No extrapolation was used in the processing of the non-uniformly sampled data and identical signal downscaling factor was used for independently processed spectra in relaxation or CEST series. The analysis and visualisation of spectra were done in the software NMRFAM-Sparky (44). In CPMG data sets signal intensities obtained from 2D spectra measured in relaxation series were converted into the effective relaxation rates $R_{2,\mathrm{eff}}$ using the Octave 3.8.2 program (45) employing the function leasqr from the package optim, by fitting peak intensities to a mono-exponential decay using a nonlinear least-squares approach:

$$I_1(\nu_{\mathrm{CPMG}}) = I_0 e^{-R_{2,\mathrm{eff}} T} \qquad [1]$$

where $\nu_{\mathrm{CPMG}} = 1/4\tau$, with 4τ being the interval between consecutive refocusing pulses of the CPMG sequence that is applied during a constant relaxation delay of duration T. $I_1(\nu_{\mathrm{CPMG}})$ and I_0 are the signal intensities in spectra measured with and without the relaxation delay T. The error in peak intensities was estimated from the random spectral noise sampled at 10 000 random positions, outside of peak regions. Uncertainties in the $R_{2,\mathrm{eff}}$ relaxation rates were determined by 2000 Monte Carlo simulation steps. Subsequently, relaxation dispersion profiles were fitted to the Carver-Richards two-site exchange model (46) using a software package GLOVE (47). The global exchange parameters, p_{B} (population of the minor state) and k_{ex} (exchange rate) were extracted by global fitting. Values of $\Delta\omega$ (chemical shift difference between the states) were extracted on the per-residue basis. Uncertainties in the exchange parameters were established by 5000 Monte Carlo simulations. The dependence of the population of the minor state p_{B} on temperature was used to obtain the change of enthalpy ΔH and entropy ΔS upon transition to the minor state following the Boltzmann's law:

$$K = \frac{p_{\mathrm{B}}}{1 - p_{\mathrm{B}}} = e^{-\frac{\Delta H - T\Delta S}{RT}}, \qquad [2]$$

where R is the molar gas constant, T is the absolute temperature, and the fraction $p_{\mathrm{B}}/(1-p_{\mathrm{B}})$ represents the equilibrium constant K.

The change of enthalpy and entropy for a transition from the ground state (ΔH_{AB} and ΔS_{AB}, respectively) or from the minor state (ΔH_{BA} and ΔS_{BA}, respectively) to a transition saddle point was determined following the Eyring equation:

$$k_{\mathrm{AB}} = p_{\mathrm{B}} k_{\mathrm{ex}} = \frac{k_B T}{h} e^{-\frac{\Delta H_{\mathrm{AB}} - T\Delta S_{\mathrm{AB}}}{RT}}, \quad [3]$$

$$k_{\mathrm{BA}} = (1-p_{\mathrm{B}}) k_{\mathrm{ex}} = \frac{k_B T}{h} e^{-\frac{\Delta H_{\mathrm{BA}} - T\Delta S_{\mathrm{BA}}}{RT}}, \quad [4]$$

where k_B is the Boltzmann's constant, h is the Planck constant, and T is the thermodynamic temperature. Errors of thermodynamic parameters were estimated using the smooth Bootstrap method.

In CEST data sets, the peak intensities were collected from 2D spectra in B_1 position series. Uncertainties in intensities were estimated in the same way as mentioned above. CEST profiles were generated and exchange parameters were extracted using the software ChemEx (48) (http://www.github.com/gbouvignies/chemex). Global/per-residue fitting as well as uncertainty estimation was done as described for the CPMG data set.

The chemical shift perturbance was calculated as

$$\Delta\omega_{\mathrm{CSP}} = \sqrt{\frac{1}{n}\sum_i (\alpha_i \Delta\omega_i)^2}, \quad [5]$$

where n was the number of available chemical shift disturbance for backbone nuclei in each residue and the parameters α_i were 0.32, 0.19, 0.12, and 1.00 for ^{13}CO, ^{13}C$^{\alpha}$, ^{15}N, and ^{1}HN nuclei, respectively.

Acknowledgements. This work was supported by Czech Science Foundation grant No. GJ18-04197Y, from European Regional Development Fund-Project MSCAfellow2@MUNI (No. CZ.02.2.69/0.0/0.0/18 070/0009846). CIISB, Instruct-CZ Centre of Instruct-ERIC EU consortium, funded by MEYS CR infrastructure project LM2018127, is gratefully acknowledged for the financial support of the measurements at the Josef Dadok National NMR Centre. LK acknowledges the project National Institute of Virology and Bacteriology (Programme EXCELES, ID Project No. LX22NPO5103) - Funded by the European Union - Next Generation EU. Authors thank Lewis Kay, Enrico Rennella, and Muhandiram Ranjiht for providing NMR pulse sequences for measurement CEST and CPMG experiments.

Author contributions. D.T. and K.B. prepared NMR samples, D.T. and P.K. measured NMR spectra, D.T., P.P., and P.K processed the spectra, D.T. and P.K. perform the analyses, D.T., L.Z., L.K., and P.K prepared the manuscript, P.K. obtained funding for the project.

Author declaration. The authors declare no conflict of interest.

Data declaration. The data that support the findings of this study are available from the corresponding author upon reasonable request.

1. Weiss A, Shaw LN. Small things considered: the small accessory subunits of RNA polymerase in gram-positive bacteria. *FEMS microbiology reviews*, 39(4):541–554, 2015.
2. Murakami KS, Darst SA. Bacterial RNA polymerases: the wholo story. *Current opinion in structural biology*, 13(1):31–39, 2003.
3. Ma C, Yang X, Kandemir H, Mielczarek M, Johnston EB, Griffith R, Kumar N, Lewis PJ. Inhibitors of bacterial transcription initiation complex formation. *ACS Chemical Biology*, 8(9):1972–1980, 2013.
4. Paget MS. Bacterial sigma factors and anti-sigma factors: structure, function and distribution. *Biomolecules*, 5(3):1245–1265, 2015.
5. Österberg S, del Peso-Santos T, Shingler V. Regulation of alternative sigma factor use. *Annual review of microbiology*, 65:37–55, 2011.
6. Bae B, Davis E, Brown D, Campbell EA, Wigneshweraraj S, Darst SA. Phage T7 Gp2 inhibition of escherichia coli RNA polymerase involves misappropriation of σ70 domain 1.1. *Proceedings of the National Academy of Sciences*, 110(49):19772–19777, 2013.
7. Murakami KS. X-ray crystal structure of $Escherichia\ coli$ RNA polymerase σ70 holoenzyme. *Journal of Biological Chemistry*, 288(13):9126–9134, 2013.
8. Zachrdla M, Padrta P, Rabatinová A, Šanderová H, Barvík I, Krásnỳ L, Žídek L. Solution structure of domain 1.1 of the σA factor from $Bacillus\ subtilis$ is preformed for binding to the RNA polymerase core. *Journal of Biological Chemistry*, 292(28):11610–11617, 2017.
9. Schwartz EC, Shekhtman A, Dutta K, Pratt MR, Cowburn D, Darst S, Muir TW. A full-length group 1 bacterial sigma factor adopts a compact structure incompatible with DNA binding. *Chemistry & biology*, 15(10):1091–1103, 2008.
10. Papoušková V, Kadeřávek P, Otrusinová O, Rabatinová A, Šanderová H, Nováček J, Krásnỳ L, Sklenář V, Žídek L. Structural study of the partially disordered full-length δ subunit of RNA polymerase from $Bacillus\ subtilis$. *ChemBioChem*, 14(14):1772–1779, 2013.
11. Purcell E.M. Carr H.Y. Effects of diffusion on free precession in nuclear magnetic resonance experiments. *Physical Review*, 94:630–638, 1954.
12. Gill D. Meiboom S. Modified spin-echo method for measuring nuclear relaxation times. *Review of Scientific Instruments*, 29:688–691, 1958.
13. Wüthrich K. NMR with proteins and nucleic acids. *Europhysics News*, 17(1):11–13, 1986.
14. Tjandra N, Bax A. Direct measurement of distances and angles in biomolecules by NMR in a dilute liquid crystalline medium. *Science*, 278(5340):1111–1114, 1997.
15. Korzhnev DM, and Kay LE. Probing invisible, low-populated states of protein molecules by relaxation dispersion NMR spectroscopy: an application to protein folding. *Accounts of Chemical Research*, 41(3):442–451, 2008.
16. Palmer 3rd AG, Kroenke CD, Loria JP. Nuclear magnetic resonance methods for quantifying microsecond-to-millisecond motions in biological macromolecules. *Methods in enzymology*, 339: 204–238, 2001.
17. Tugarinov V, Kay LE. Methyl groups as probes of structure and dynamics in NMR studies of high-molecular-weight proteins. *ChemBioChem*, 6(9):1567–1577, 2005.
18. Haigh CW, Mallion RB. Ring current theories in nuclear magnetic resonance. *Progress in nuclear magnetic resonance spectroscopy*, 13(4):303–344, 1979.
19. Berjanskii MV, Wishart DS. A simple method to predict protein flexibility using secondary chemical shifts. *Journal of the American Chemical Society*, 127(43):14970–14971, 2005.
20. Marsh JA, Singh VK, Jia Z, Forman-Kay JD. Sensitivity of secondary structure propensities to sequence differences between α-and γ-synuclein: Implications for fibrillation. *Protein Science*, 15 (12):2795–2804, 2006.
21. Salmon L, Nodet G, Ozenne V, Yin G, Malene Ringkjøbing Jensen, Markus Zweckstetter, and Martin Blackledge. NMR characterization of long-range order in intrinsically disordered proteins. *Journal of the American Chemical Society*, 132(24):8407–8418, 2010.

22. Sekhar A, Kay LE. NMR paves the way for atomic level descriptions of sparsely populated, transiently formed biomolecular conformers. *Proceedings of the National Academy of Sciences*, 110(32): 12867–12874, 2013.
23. Alderson TR, Kay LE. Unveiling invisible protein states with NMR spectroscopy. *Current opinion in structural biology*, 60:39–49, 2020.
24. Pletnev P, Pupov D, Pshanichnaya L, Esyunina D, Petushkov I, Nesterchuk M, Osterman I, Rubtsova M, Mardanov A, Ravin N, Sergiev P, Kulbachinskiy A, Dontsova O. Rewiring of growth-dependent transcription regulation by a point mutation in region 1.1 of the housekeeping σ factor. *Nucleic acids research*, 48(19):10802–10819, 2020.
25. Patel UR, Gautam S, Chatterji D. Validation of omega subunit of RNA polymerase as a functional entity. *Biomolecules*, 10(11):1588, 2020.
26. Shin Y, Qayyum MZ, Pupov D, Esyunina D, Kulbachinskiy A, Murakami KS. Structural basis of ribosomal RNA transcription regulation. *Nature Communications*, 12:528, 2021.
27. Kerfah R, Plevin MJ, Sounier R, Gans P, Boisbouvier J. Methyl-specific isotopic labeling: a molecular tool box for solution nmr studies of large proteins. *Current Opinion in Structural Biology*, 32: 113–122, 2015.
28. Gans P, Hamelin O, Sounier R, Ayala I, Durá MA, Amero CD, Noirclerc-Savoye M, Franzetti B, Plevin MJ, Boisbouvier J. Stereospecific isotopic labeling of methyl groups for NMR spectroscopic studies of high-molecular-weight proteins. *Angewandte Chemie*, 122(11):2002–2006, 2010.
29. Lundström P, Teilum K, Carstensen T, Bezsonova I, Wiesner S, Hansen DF, Religa TL, Akke M, Kay LE. Fractional ^{13}C enrichment of isolated carbons using [1-^{13}C]-or [2-^{13}C]-glucose facilitates the accurate measurement of dynamics at backbone C$^{\alpha}$ and side-chain methyl positions in proteins. *Journal of biomolecular NMR*, 38(3):199–212, 2007.
30. Loria JP, Rance M, Palmer AG. A relaxation-compensated Carr-Purcell-Meiboom-Gill sequence for characterizing chemical exchange by NMR spectroscopy. *Journal of the American Chemical Society*, 121(10):2331–2332, 1999.
31. Yip GNB, Zuiderweg ERP. A phase cycle scheme that significantly suppresses offset-dependent artifacts in the R2-CPMG ^{15}N relaxation experiment. *Journal of Magnetic Resonance*, 171(1): 25–36, 2004.
32. Vallurupalli P, Hansen DF, Stollar E, Meirovitch E, Kay LE. Measurement of bond vector orientations in invisible excited states of proteins. *Proceedings of the National Academy of Sciences*, 104 (47):18473–18477, 2007.
33. Hansen MR, Hanson P, Pardi A. Filamentous bacteriophage for aligning RNA, DNA, and proteins for measurement of nuclear magnetic resonance dipolar coupling interactions. *Methods in enzymology*, 317:220–240, 2000.
34. Rückert M, Otting G. Alignment of biological macromolecules in novel nonionic liquid crystalline media for nmr experiments. *Journal of the American Chemical Society*, 122(32):7793–7797, 2000.
35. Ottiger M, Delaglio F, Bax A. Measurement of J and dipolar couplings from simplified two-dimensional NMR spectra. *Journal of Magnetic Resonance*, 131(2):373–378, 1998.
36. Kay LE, Vallurupalli P, Bouvignies G. Studying "invisible" excited protein states in slow exchange with a major state conformation. *Journal of the American Chemical Society*, 134:8184–8161, 2012.
37. Kay LE, Bouvignies G, Vallurupalli P. Visualizing side chains of invisible protein conformers by solution nmr. *Journal of Molecular Biology*, 426:763–774, 2014.
38. Kay LE, Long D, Sekhar A. Triple resonance-based ^{13}C$^{\alpha}$ and ^{13}C$^{\beta}$ CESTR experiments for studies of ms timescale dynamics in proteins. *Journal of biomolecular NMR*, 60:203–208, 2014.
39. Kay LE, Vallurupalli P. Probing slow chemical exchange at carbonyl sites in proteins by chemical exchange saturation transfer NMR. *Angewandte Chemie*, 52:4156–4159, 2013.
40. Yuwen T, Bouvignies G, Kay LE. Exploring methods to expedite the recording of CEST datasets using selective pulse excitation. *Journal of Magnetic Resonance*, 292:1–7, 2018.
41. Baldwin AJ, Hansen DF, Vallurupalli P, Kay LE. Measurement of methyl axis orientations in invisible, excited states of proteins by relaxation dispersion NMR spectroscopy. *Journal of the American Chemical Society*, 131:11939–11948, 2009.
42. Kay Lewis E. Skrynnikov N.R., Dahlquist F.W. Reconstructing NMR spectra of "invisible" excited protein states using HSQC and HMQC experiments. *Journal of the American Chemical Society*, 124:12352–12360, 2002.
43. Delaglio F, Grzesiek S, Vuister GW, Zhu G, Pfeifer J, Bax A. NMRPipe: a multidimensional spectral processing system based on UNIX pipes. *Journal of biomolecular NMR*, 6(3):277–293, 1995.
44. Lee W, Tonelli M, Markley JL. NMRFAM-SPARKY: enhanced software for biomolecular NMR spectroscopy. *Bioinformatics*, 31(8):1325–1327, 2015.
45. Eaton JW, Bateman D, Hauberg S. *GNU Octave version 3.0. 1 manual: a high-level interactive language for numerical computations*. SoHo Books, 2007.
46. Carver JP, Richards RE. A general two-site solution for the chemical exchange produced dependence of T_2 upon the carr-Purcell pulse separation. *Journal of Magnetic Resonance (1969)*, 6(1): 89–105, 1972.
47. Sugase K, Konuma T, Lansing JC, Wright PE. Fast and accurate fitting of relaxation dispersion data using the flexible software package GLOVE. *Journal of biomolecular NMR*, 56(3):275–283, 2013.
48. Vallurupalli P, Bouvignies G, Kay LE. Studying "invisible" excited protein states in slow exchange with a major state conformation. *Journal of the American Chemical Society*, 134(19):8148–8161, 2012.